

## Multiferroic response and clamped domain structure in a two-dimensional spiral magnet: Monte Carlo simulation

Qichang Li, Shuai Dong, and J.-M. Liu\*

*Laboratory of Solid State Microstructure, Nanjing University, Nanjing 210093, China**and International Center for Materials Physics, Chinese Academy of Sciences, Shenyang 110015, China*

(Received 5 November 2007; revised manuscript received 7 January 2008; published 29 February 2008)

The Monte Carlo simulation on multiferroic behaviors of the two-dimensional  $\text{MnO}_2$  lattice in multiferroic manganites is performed based on the model [I. A. Sergienko and E. Dagotto, Phys. Rev. B **73**, 094434 (2006)] associated with the Dzyaloshinskii-Moriya interaction. The simulated ferroelectric polarization induced by the spiral spin ordering and its response to external magnetic field agree well with reported experimental observations. Furthermore, the coexistence of clamped ferroelectric domains and spiral spin domains is revealed in our simulation.

DOI: [10.1103/PhysRevB.77.054442](https://doi.org/10.1103/PhysRevB.77.054442)

PACS number(s): 75.80.+q, 77.80.Bh, 75.30.Kz, 77.80.Dj

Research interest in multiferroics with coexisting ferroelectric (FE) and ferromagnetic (FM) or antiferromagnetic (AFM) orderings has been revived recently due to their promising technological potentials in storage devices and sensors.<sup>1-3</sup> In the past few years, the gigantic magnetoelectric (ME) effect, that is, FE polarization  $P$  of the order of magnitude of  $\sim 1.0 \mu\text{C}/\text{cm}^2$  or less, was observed in perovskite manganites such as  $\text{RMnO}_3$  ( $R=\text{Tb, Dy, and Gd}$ ),<sup>4-6</sup>  $\text{RMn}_2\text{O}_5$  ( $R=\text{Y, Tb, Dy, Ho, Er, etc.}$ ),<sup>7-9</sup> and kagomé-lattice compound  $\text{Ni}_3\text{V}_2\text{O}_8$ .<sup>10,11</sup> Huge efforts from both experimentalists and theorists have been made to understand the new mechanism underlying this effect. At least for some multiferroic manganites such as  $\text{TbMnO}_3$ , a spiral-spin configuration might play an important role in generating the FE polarization,<sup>6,12</sup> and a change in the magnetic structure at the FE Curie point  $T_c$ , where  $P$  is initiated, was demonstrated by neutron diffraction.<sup>13,14</sup> The magnetic symmetry consideration also suggested a transition from sinusoidal (collinear) spin order to spiral (noncollinear) spin order near  $T_c$ .<sup>14</sup> On the other hand, the microscopic origin for this FE order, as proposed by Katsura *et al.*,<sup>15</sup> is related to the Mn-O-Mn bond structure, in which an overlap of the wave functions between the two adjacent  $3d$  Mn ions with canted-spin arrangement favors a small polarization due to the displacement of the sandwiched oxygen ion. Subsequently, it was suggested that transverse-spiral spin modulation along a specific direction could induce a macroscopic FE polarization.<sup>16,17</sup>

The possible form of exchange interactions responsible for the spiral-spin-induced ferroelectricity was proposed in several models. Sergienko and Dagotto addressed the significance of the antisymmetric Dzyaloshinskii-Moriya interaction (DMI) in the appearance of the FE ordering for rare-earth perovskite  $\text{RMnO}_3$ . In this model, a ME coupling term  $\mathbf{D} \cdot (\mathbf{S}_i \times \mathbf{S}_j)$ , where  $\mathbf{D}$  is a vector correlating to the displacement of the oxygen ion between moments  $\mathbf{S}_i$  and  $\mathbf{S}_j$ , is included.<sup>18</sup> Harris *et al.* proposed a more complicated theory to explain the ME effect in  $\text{Ni}_3\text{V}_2\text{O}_8$ , in which an exchange tensor is introduced to include the contributions from the superexchange, double exchange, and DMI between the nearest neighboring moments.<sup>19</sup> Mostovoy developed a phenomenological theory for inhomogeneous multiferroics, where the ME effect is associated with the spatial derivatives of magnetic moment.<sup>20</sup>

Although preliminary calculations based on the above models highlighted the major features associated with the ME response, more detailed investigations on the interplay between the FE and magnetic orders, in the quantitative sense, would be helpful to illustrate this fantastic effect. Although nonzero  $P$  under zero magnetic field, induced at an incommensurate magnetic (ICM) transition, was revealed by Monte Carlo (MC) simulation,<sup>18</sup> yet the detailed dependence of  $P$  on magnetic field  $H$  has not been reported. In fact, as far as we know, few works on the MC simulation of such effect have been reported.

To perform a MC simulation, one needs to understand the interactions between order parameters. Raman study indicates that the in-plane oxygen vibrations are mainly involved in the spin-phonon coupling in orthorhombic  $\text{RMnO}_3$  ( $R=\text{Tb and Dy}$ ).<sup>21</sup> Although the  $ab$  planes of these materials are antiferromagnetically stacked along the  $c$  axis,<sup>14</sup> the direction of induced  $P$  is identical in these  $ab$  planes. It is, therefore, a worthwhile attempt to study the ME effect of a two-dimensional (2D) system in which the oxygen movements are limited within a plane. The spins coupled with the O displacements are treated as in-plane too. Surely, it does not mean that the spins of Mn ion in  $\text{RMnO}_3$  are limited within one specific plane. However, one can project the spins onto a plane, which will not lose the physical essence.<sup>14</sup> We start from the DMI model developed by Sergienko and Dagotto<sup>18</sup> and perform a detailed calculation of the dependence of  $P$  on  $H$ . The calculated results will be compared with recent experiments. We further demonstrate how the FE domains and magnetic domains are interactively clamped, illustrating the microscopic pictures of the ME effect in multiferroics.

The MC simulation is performed on a 2D  $L \times L$  square lattice with periodic boundary conditions, representing the  $\text{MnO}_2$  plane of multiferroic  $\text{RMnO}_3$ . The plane is schematically illustrated in Fig. 1(a), where each Mn ion (blue dot) is surrounded by four O ions (red dots). The magnetization  $M$  is assumed from the contribution of the Mn spins, and  $P$  is attributed to the displacement of O ions. Both of them are restricted within the  $xy$  (or  $ab$ ) plane. For such a lattice, we directly take the original Hamiltonian<sup>18</sup> based on the orbitally degenerate double-exchange model:

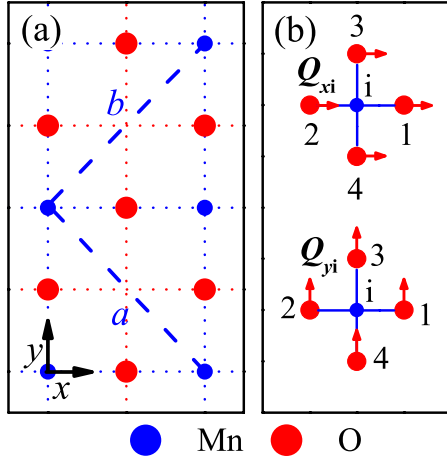


FIG. 1. (Color online) (a) Two-dimensional  $\text{MnO}_2$  lattice for the MC simulation, and (b) the FE classical phonon modes associated with the displacements of oxygen ions.

$$\begin{aligned} \tilde{H} = & - \sum_{i\alpha\beta\sigma} t_{\alpha\beta}^{\alpha} d_{i\alpha\sigma}^{\dagger} d_{i+\alpha\beta\sigma} - J_H \sum_{ia} S_i \cdot S_i + J_{AF} \sum_{ia} S_i \cdot S_{i+a} \\ & - \mu_B g_L \sum_i H \cdot S_i + \sum_i 2eE \cdot r_i + \sum_{ia} D^a(r_i) \cdot [S_i \times S_{i+a}] \\ & + \frac{\kappa_1}{2} \sum_i (Q_{xi}^2 + Q_{yi}^2) + H_{JT} + \frac{\kappa_2}{2} \sum_i \sum_m Q_{mi}^2, \end{aligned} \quad (1)$$

where  $d_{i\alpha\sigma}^{\dagger}$  is the creation operator for the electron carrying spin  $\sigma$  on site  $i$ , and  $t_{\alpha\beta}^{\alpha}$  is the hopping integral.  $J_H$  is the Hund coupling constant between the  $e_g$  electrons with spin  $S_i$  and three  $t_{2g}$  electrons with a classical spin  $S_i=1.4$  in moment.<sup>14,18</sup>  $J_{AF}$  represents the AFM isotropic superexchange between  $t_{2g}$  spins,  $H$  denotes the external magnetic field,  $\mu_B$  is the Bohr magnon,  $g_L$  represents the Lande factor,  $E$  denotes a small electric field,  $e$  is the charge of the electron,  $r_i$  represents the O displacement, and  $D^a(r_i)$  is a vector concerning the displacement of O ions and scaling the magnitude of the DMI.  $Q_{xi}$  and  $Q_{yi}$  denote the classical FE phonon coordinates [shown in Fig. 1(b), also referring to Ref. 18] along the  $x$  and  $y$  axes, respectively, associated with the displacement of the four O ions surrounding the Mn site  $i$ , while  $Q_{mi}$  represents the remnant phonon coordinates. Finally,  $\kappa_1$  and  $\kappa_2$  denote the spring constants of the FE modes and the remnant modes, and  $H_{JT}$  is the term from the Jahn-Teller (JT) distortion.

For the  $ab$  plane,  $D^a(r_i)$  in the  $x$  and  $y$  directions takes the following forms:<sup>18</sup>

$$D^x(r_i) = \gamma(0, 0, y_i), \quad D^y(r_i) = \gamma(0, 0, -x_i), \quad (2)$$

where  $\gamma$  is a constant scaling the coupling intensity between the spins and the displacements. Term  $H_{JT}$  is redefined to fit the 2D model, based on the three-dimensional form:<sup>22,23</sup>

$$H_{JT} = \lambda(q_{1i}\rho_i + q_{2i}\tau_{xi} + q_{3i}\tau_{zi}) + \frac{1}{2} \sum_i (2q_{1i}^2 + q_{2i}^2 + q_{3i}^2), \quad (3)$$

where  $\rho_i$  and  $\tau_i$  are the orbital pseudospins, and  $q_{1i}$ ,  $q_{2i}$ , and  $q_{3i}$  represent the JT breath modes and the stretch modes. For

TABLE I. Parameters chosen for the simulation.

Parameter	Value	Parameter	Value
$k_B$ (J/K)	$1.3807 \times 10^{-23}$	$\gamma/k_B$ (K/Å)	$1.5 \times 10^3$
$\mu_B$ (J/T)	$9.274 \times 10^{-24}$	$\kappa_1$ (K/Å <sup>2</sup> )	$1.0 \times 10^5$
$g_L$	2	$\kappa_2$ (K/Å <sup>2</sup> )	$1.0 \times 10^6$
$J_{AF}/k_B$ (K)	2		

simplicity, the contribution of the  $e_g$  electrons is not considered, referring to highly localized manganites. Hence, the first two terms of Eq. (1) and the first term of Eq. (3) are simply discarded. The exclusion of these terms is physically acceptable since it has been proven that both the double exchange and superexchange between noncollinear spins are able to induce the FE polarization.<sup>15</sup>

For subsequent comparison with experiments, we highlight the choice of the parameters taken for our simulation (Table I). The reported Curie temperature  $T_c$  of  $\text{DyMnO}_3$  and  $\text{TbMnO}_3$  is of the order of 10 K. The value of  $P$  ranges from 0.08 to 0.25  $\mu\text{C}/\text{cm}^2$ .<sup>4,5</sup> Hence the derived magnitude of the FE phonon coordinate  $Q$  is of the order of  $10^{-3}$ – $10^{-2}$  Å. Following the routine of Zhou and Goodenough,<sup>24</sup>  $\kappa_1 = k_B T_c / Q^2$ , which gives  $\kappa_1/k_B \sim 10^5$  K/Å<sup>2</sup> with  $Q \sim 10^{-2}$  Å; here,  $k_B$  denotes the Boltzmann constant.  $\kappa_2 = 10\kappa_1$  is taken so that the system favors the ICM-FE phase. Considering the difference of the Néel temperature between  $\text{LaMnO}_3$  (Refs. 25 and 26) and  $\text{RMnO}_3$  ( $R=\text{Dy}$  and  $\text{Tb}$ ),  $J_{AF}/k_B=2$  K is a reasonable choice.  $D(r_i)/k_B=15$  K is chosen in order to tune the ICM transition point ( $\sim 12$  K in this work) to fit the experimental value. Correspondingly,  $\gamma=1.5 \times 10^3$  K/Å in our simulation. It is noticed that  $D(r_i)$  is about 1 order of magnitude larger than the estimated value for  $\text{LaMnO}_3$ .<sup>25,26</sup> However, this discrepancy may be diminished when the model is improved, as illustrated in previous work.<sup>18</sup>

The details of the simulation procedure are the same as reported earlier.<sup>18</sup> For every temperature  $T$  in the  $P$ - $T$  and  $M$ - $T$  curves, initial 12 500 Monte Carlo steps (MCSs) are discarded for equilibration and 47 500 MCSs retained for average. For every specific  $H$  in the  $P$ - $H$  and  $M$ - $H$  curves, initial 500 MCSs are discarded and 1500 MCSs retained for average. The Mn spin and O displacement are updated according to the Metropolis algorithm, with the displacement restricted between  $-10 \times 10^{-2}$  and  $10 \times 10^{-2}$  Å in the updating process.

According to the previous report,<sup>18</sup>  $P$  along a specific direction ( $b$  axis) is induced due to the ICM phase transition in the 2D lattice. Nevertheless, given the fourfold symmetry of the lattice, four possible directions of  $P$  (parallel and antiparallel to  $a$  axis and  $b$  axis, respectively) corresponding to four types of spiral-spin configuration are, in fact, allowed with equal possibility. We present here in Figs. 2(a)–2(d) all four types of ICM-FE configurations which are achieved by applying a small  $E$  parallel to one of the allowed directions. It is somehow equivalent to the experimental poling procedure. As a result, the fourfold symmetry is broken and only one direction of  $P$  is favored over the lattice. Due to the DMI term in Eq. (1), the uniquely oriented  $P$  helps to stabilize a specific spiral spin configuration, characterized by a wave

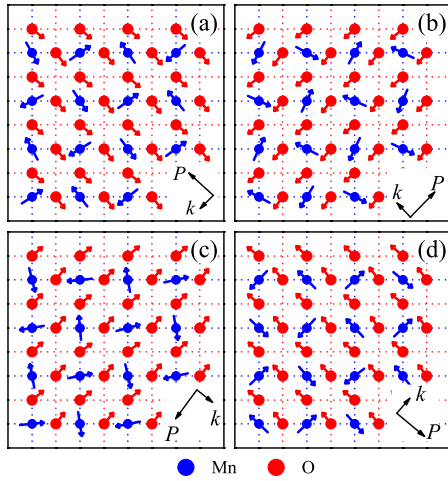


FIG. 2. (Color online) Snapshots for four types of the spiral spin and FE dipole structure of a  $4 \times 4$  cluster at  $T=0.01$  K. The Mn and O ions are located at the sites of the  $\text{MnO}_2$  layer of the ideal cubic perovskite lattice. Spin of Mn ions and displacement of O ions are denoted by blue and red arrows, respectively.

vector  $k$  normal to  $P$ , which points to the direction along which the noncollinear spins rotate clockwise. For each configuration shown in Fig. 2,  $E$  ( $Ee/k_B=30$  K/Å) is applied parallel to  $P$ . Unless stated otherwise, our simulations are performed with  $Ee/k_B=30$  K/Å applied along the  $b$  axis. This field is  $\sim 10^2$  kV/cm, on the same order of magnitude with experimentally employed value for poling ferroelectric oxide ceramics at low  $T$ .

Figures 3(a) and 3(b) present the simulated  $M$  and  $P$  as a function of  $T$  under various  $H$  ( $H \parallel a$ ), for both cooling and heating sequences. In this paper,  $M$  is the average of spins over the lattice and  $P$  is equal to the averaged dipole moment divided by the cell volume of  $\text{DyMnO}_3$ . It is shown that under  $H=0$ , the lattice exhibits almost zero  $M$  over the whole  $T$  range, while a clear FE transition occurs at  $T=T_c$

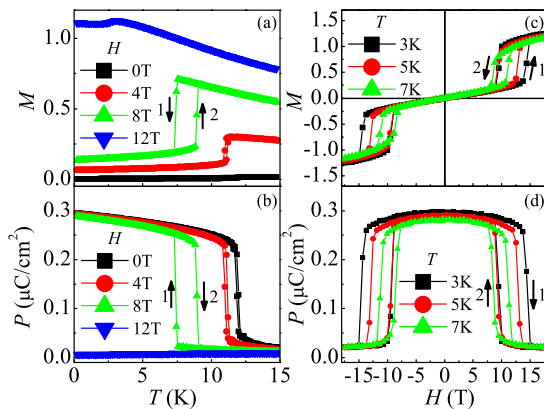


FIG. 3. (Color online) (a) Magnetization  $M$  and (b) polarization  $P$  as a function of  $T$  at various  $H$ , and (c)  $M$  and (d)  $P$  as a function of  $H$  at different  $T$ . The up arrow and down arrow in (a) and (b) denote the heating and cooling sequences, respectively, and those in (c) and (d) denote the varying paths of  $H$ . Numbers in the figure denote the sequence of the MC simulations.

$\sim 12$  K, at which a transition from the paramagnetic state to the ICM phase (as shown in Fig. 2) is identified. The sudden flop of  $P$  and the weak but clear thermal hysteresis indicate the first order FE transition here. For the cases of  $H>0$ ,  $T_c$  shifts toward the low- $T$  side with increasing  $H$ . Upon further increasing  $H$  up to 12 T, the ICM configuration collapses into the spin-canted weak FM state. Since such a spin order does not favor the FE order, we observe the disappearance of  $P$  over the whole  $T$  range.

We present in Figs. 3(c) and 3(d) the  $H$  dependence of  $M$  and  $P$  at several selected  $T$  ( $T_s=3, 5$ , and  $7$  K, respectively) below  $T_c$ . The simulation is performed as follows. The lattice is first cooled from  $T=40$  K down to  $T_s$  ( $T_s=3, 5$ , and  $7$  K, respectively) under  $H=-18$  T, and then  $H$  is cycled between  $H=18$  T and  $H=-18$  T. The response of  $M$  and  $P$  to varying  $H$  is featured by the double-loop hysteresis. The steep steps of the hysteresis in Fig. 3(c) represent, respectively, the destruction (up arrow) and construction (down arrow) of the spiral-spin configuration. In response to the destruction (construction),  $P$  becomes suppressed (resumed). When  $T_s$  is higher, the critical field  $H_c$  for the destruction (construction) becomes lower, and the loop area for the  $M$ - $H$  and  $P$ - $H$  hysteresis loops shrinks.

If the ICM transition point at  $H=0$  is adjusted to  $\sim 12$  K, comparable to the so-called lock-in temperature of  $\text{DyMnO}_3$  ( $\sim 20$  K) (Ref. 5) and  $\text{TbMnO}_3$  ( $\sim 28$  K),<sup>4</sup> the simulated maximal  $P$  is  $\sim 0.3$   $\mu\text{C}/\text{cm}^2$  (Fig. 3), in good agreement with the measured value in  $\text{DyMnO}_3$ .<sup>5</sup> The thermal hysteresis illustrated in Fig. 3 was also reported experimentally.<sup>4,5</sup> The simulated minimal  $H$  required for the suppression of  $P$  is about 12 T, a little larger than the experimental value ( $\sim 5$ – $9$  T) for  $\text{DyMnO}_3$  and  $\text{TbMnO}_3$ , but still in a comparable range.

The simulated results presented above refer to the response of uniquely oriented  $P$  to  $H$  at different temperatures. However, at  $E=0$ , four equivalent directions of  $P$  are allowed; it is, therefore, reasonable to expect that the FE domains and spin-ordered domains coexist and interactively clamped owing to the strong mutual influence between the FE and magnetic orders. To illustrate this feature, we perform the simulation under zero  $E$ . First, the lattice is cooled from  $T=40$  K to  $T=0.01$  K under zero  $H$  and  $E$ , and then  $H$  increases gradually to  $H=18$  T in the isothermal condition. As shown in Fig. 4(a),  $P$  is gradually suppressed (path 1) down to zero around  $H \sim 13$  T. Nevertheless, upon subsequent decrease of  $H$  from  $H=18$  T down to zero,  $P$  does not return back to the initial state but evolves along path 2 with  $P=0$ . The reason behind this anomaly is the existence of the  $90^\circ$  FE domains in the lattice compatible with the spiral-spin-ordered regions, as shown in Fig. 4(c). The directions of  $P$  are normal to each other between the adjacent domains, and opposite between the cross domains. Hence, the macroscopic FE polarization remains zero. The wave vectors for the local spin ordered regions associated with the FE domains exhibit similar characters. If one defines the magnetic domains by the wave vector, one may find that the magnetic domain walls are coincident with the FE ones. In other words, they are mutually clamped owing to the strong ME coupling. In addition, the  $180^\circ$  FE domains are observed in this work, although they are not shown here.

As shown above, the formation of multiferroic domains

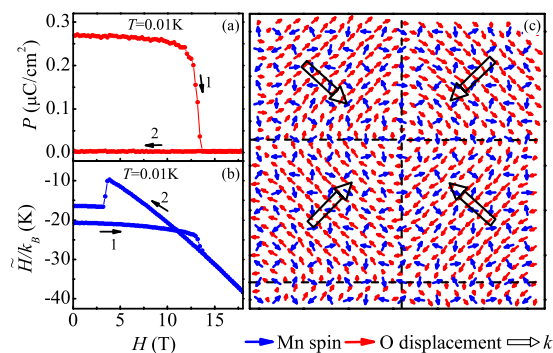


FIG. 4. (Color online)  $H$ -dependence of (a)  $P$  and (b) average Hamiltonian per site at  $T=0.01\text{ K}$ . (c) Typical snapshot of the  $90^\circ$  domains separated by dashed lines. Numbers in (a) and (b) denote the sequence of the MC simulations.

can be realized in a properly designed system. Actually, observation of the clamped FE domains and magnetic domains has been reported in recent work on multiferroic manganites.<sup>27</sup> The MC simulation provides an extra proof for the experimental observation. For the present system, due to the fourfold symmetry, both the  $90^\circ$  and  $180^\circ$  domains are

allowed, while different domain configurations may be possible depending on the symmetry of the system. The metastability of the multidomain configuration in this work, evidenced by Fig. 4(b), is attributed to the exclusion of the depolarization energy in our simulation, which can be lowered by the formation of a domain structure in compensation of the increase of the domain wall energy.

In conclusion, we have simulated the presence of FE polarization in a 2D noncollinear multiferroic lattice as a result of the DM interaction. The response of the FE polarization and magnetization to external magnetic field at different temperatures has been investigated. The simulation results reveal that the FE polarization relies essentially on the spiral-spin structure. Given the sufficiently high magnetic field, the FE polarization may be destroyed due to the broken spiral-spin configuration. The interactively clamped FE domains and spiral-spin domains are demonstrated in this simple model system. The gigantic ME effect as demonstrated is in good agreement with previous experiments.

We thank the Natural Science Foundation of China (No. 50601013 and No. 10674061) and National Key Projects for Basic Research of China (No. 2002CB613303 and No. 2006CB921802).

\*Author to whom any correspondence should be addressed; liujm@nju.edu.cn

<sup>1</sup>M. Fiebig, J. Phys. D **38**, R123 (2005).

<sup>2</sup>J. F. Scott, Nat. Mater. **6**, 256 (2007).

<sup>3</sup>W. Eerenstein, N. D. Mathur, and J. F. Scott, Nature (London) **442**, 759 (2006).

<sup>4</sup>T. Kimura, T. Goto, H. Shintani, K. Ishizaka, T. Arima, and Y. Tokura, Nature (London) **426**, 55 (2003).

<sup>5</sup>T. Goto, T. Kimura, G. Lawes, A. P. Ramirez, and Y. Tokura, Phys. Rev. Lett. **92**, 257201 (2004).

<sup>6</sup>T. Arima, T. Goto, Y. Yamasaki, S. Miyasaka, K. Ishii, M. Tsubota, T. Inami, Y. Murakami, and Y. Tokura, Phys. Rev. B **72**, 100102(R) (2005).

<sup>7</sup>N. Hur, S. Park, P. A. Sharma, J. S. Ahn, S. Guha, and S. W. Cheong, Nature (London) **429**, 392 (2004).

<sup>8</sup>L. C. Chapon, P. G. Radaelli, G. R. Blake, S. Park, and S. W. Cheong, Phys. Rev. Lett. **96**, 097601 (2006).

<sup>9</sup>D. Higashiyama, S. Miyasaka, and Y. Tokura, Phys. Rev. B **72**, 064421 (2005).

<sup>10</sup>G. Lawes, A. B. Harris, T. Kimura, N. Rogado, R. J. Cava, A. Aharony, O. Entin-Wohlman, T. Yildirim, M. Kenzelmann, C. Broholm, and A. P. Ramirez, Phys. Rev. Lett. **95**, 087205 (2005).

<sup>11</sup>K. Taniguchi, N. Abe, T. Takenobu, Y. Iwasa, and T. Arima, Phys. Rev. Lett. **97**, 097203 (2006).

<sup>12</sup>T. Arima, A. Tokunaga, T. Goto, H. Kimura, Y. Noda, and Y. Tokura, Phys. Rev. Lett. **96**, 097202 (2006).

<sup>13</sup>R. Kajimoto, H. Yoshizawa, H. Shintani, T. Kimura, and Y. Tokura, Phys. Rev. B **70**, 012401 (2004).

<sup>14</sup>M. Kenzelmann, A. B. Harris, S. Jonas, C. Broholm, J. Schefer, S. B. Kim, C. L. Zhang, S. W. Cheong, O. P. Vajk, and J. W. Lynn, Phys. Rev. Lett. **95**, 087206 (2005).

<sup>15</sup>H. Katsura, N. Nagaosa, and A. V. Balatsky, Phys. Rev. Lett. **95**, 057205 (2005).

<sup>16</sup>Y. Yamasaki, S. Miyasaka, Y. Kaneko, J. P. He, T. Arima, and Y. Tokura, Phys. Rev. Lett. **96**, 207204 (2006).

<sup>17</sup>Y. Tokura, Science **312**, 1481 (2006).

<sup>18</sup>I. A. Sergienko and E. Dagotto, Phys. Rev. B **73**, 094434 (2006).

<sup>19</sup>A. B. Harris, T. Yildirim, A. Aharony, and O. Entin-Wohlman, Phys. Rev. B **73**, 184433 (2006).

<sup>20</sup>M. Mostovoy, Phys. Rev. Lett. **96**, 067601 (2006).

<sup>21</sup>J. Laverdiere, S. Jandl, A. A. Mukhin, V. Y. Ivanov, V. G. Ivanov, and M. N. Iliev, Phys. Rev. B **73**, 214301 (2006).

<sup>22</sup>E. Dagotto, T. Hotta, and A. Moreo, Phys. Rep. **344**, 1 (2001).

<sup>23</sup>T. Hotta, M. Moraghebi, A. Feiguin, A. Moreo, S. Yunoki, and E. Dagotto, Phys. Rev. Lett. **90**, 247203 (2003).

<sup>24</sup>J. S. Zhou and J. B. Goodenough, Phys. Rev. Lett. **96**, 247202 (2006).

<sup>25</sup>M. Tovar, G. Alejandro, A. Butera, A. Caneiro, M. T. Causa, F. Prado, and R. D. Sánchez, Phys. Rev. B **60**, 10199 (1999).

<sup>26</sup>F. Moussa, M. Hennion, J. Rodriguez-Carvajal, H. Moudden, L. Pinsard, and A. Revcolevschi, Phys. Rev. B **54**, 15149 (1996).

<sup>27</sup>M. Fiebig, T. Lottermoser, D. Fröhlich, A. V. Goitsev, and R. V. Pisarev, Nature (London) **419**, 818 (2002).